Chemical Science

ROYAL SOCIETY OF CHEMISTRY

EDGE ARTICLE

View Article Online
View Journal | View Issue

Cite this: *Chem. Sci.*, 2021, **12**, 7727

All publication charges for this article have been paid for by the Royal Society of Chemistry

Synthesis of an AIEgen functionalized cucurbit[7]uril for subcellular bioimaging and synergistic photodynamic therapy and supramolecular chemotherapy†

Jia Chen,[a] Shengke Li,[bc] Zeyu Wang,[a] Yating Pan,[c] Jianwen Wei,[a] Siyu Lu,[d] Qing-Wen Zhang,[a] Lian-Hui Wang[c] and Ruibing Wang *[a]

Received 26th February 2021
Accepted 21st April 2021

DOI: 10.1039/d1sc01139a

rsc.li/chemical-science

Aggregation-induced emission (AIE) based fluorophores (AIEgens) have attracted increasing attention for biomedical applications due to their unique optical properties. Here we report an AIE photosensitizer functionalized CB[7], namely AIECB[7], which could spontaneously self-assemble into nanoaggregates in aqueous solutions. Interestingly, the carbonyl-lace of CB[7] may potentially act as a proton acceptor in an acidic environment to fine-tune the fluorescence and singlet oxygen generation of AIECB[7] nanoaggregates by regulating the inner stacking of AIEgens. Additionally, benefiting from the guest-binding properties of CB[7], oxaliplatin was included into AIECB[7] nanoaggregates for combined photodynamic therapy and supramolecular chemotherapy. To show the modular versatility of this supramolecular system, a hypoxia-activatable prodrug banoxantrone (AQ4N) was loaded into AIECB[7] nanoaggregates, which exhibited synergistic antitumor effects on a multicellular tumor spheroid model (MCTS). This work not only provides AIECB[7] for versatile theranostic applications, but also offers important new insights into the design and development of macrocycle-conjugated AIE materials for diverse biomedical applications.

Introduction

In recent years, aggregation induced emission fluorophores (AIEgens) have aroused great interest in biomedical applications due to their unique fluorescence properties.[1–3] Compared with traditional fluorophores that often suffer from aggregation-caused quenching (ACQ) in an aggregation state, AIEgens exhibit higher photobleaching resistance and superior high-concentration applicability as bioprobes, and more efficient photosensitizing properties as photosensitizers for imaging guided photodynamic therapy (PDT).[1,2] Through delicate design, covalent or noncovalent conjugation of AIEgens with other functional motifs often yields multifunctional AIEgen-based hybrid materials with improved and tunable AIE properties for various biomedical applications.[4,5] In particular, the integration of host–guest properties with AIEgens may provide a facile strategy to modulate their photophysical and photochemical properties *via* direct host–guest complexation.[3,6,7] Recently, Ding *et al.* reported the inhibition of the intersystem crossing and thermal deactivation dissipation pathways of AIEgens upon host–guest complexation with calixarene, which minimized their phototoxicity and maximized the conversion of excitation energy to fluorescence emission during bioimaging.[8] Huang *et al.* developed adaptive AIEgen photosensitizers *via* host–guest complexation of AIEgens with pillararenes, to realize site-specific activation in an acidic tumor environment.[9] Moreover, Cao *et al.* fabricated supramolecular organic frameworks (SOFs) with a controllable shape and tunable luminescence through cucurbit[8]uril-mediated homo/hetero-host–guest complexation of AIEgen derivatives for cellular imaging.[10,11] Despite these successes where the properties of AIEgens are controlled *via* direct host–guest interactions, no additional guest drugs can be loaded into these systems for imaging-guided synergistic therapy. The covalent conjugation of AIEgens with macrocycles to integrate the AIEgen-based bioimaging guided photodynamic therapy with supramolecular chemotherapy mediated by host–guest complexation of drug molecules has never been reported.

[a]*State Key Laboratory of Quality Research in Chinese Medicine, Institute of Chinese Medical Sciences, University of Macau, Taipa, Macau, 999078, China. E-mail: rwang@um.edu.mo*

[b]*School of Materials Science and Engineering, Nanjing University of Science and Technology, Nanjing, 210094, China*

[c]*Key Laboratory for Organic Electronics and Information Displays, Institute of Advanced Materials, Nanjing University of Posts and Telecommunications, 9 Wenyuan Road, Nanjing, 210023, China*

[d]*Green Catalysis Center, College of Chemistry and Molecular Engineering, Zhengzhou University, 100 Kexue Road, Zhengzhou, 450001, China*

† Electronic supplementary information (ESI) available. See DOI: 10.1039/d1sc01139a

Cucurbit[*n*]urils (CB[*n*]s, $n = 5$–8, 10, 14) are a unique family of pumpkin-shaped macrocyclic host molecules that have been well demonstrated as a superior "intermediary" for both bioimaging and chemotherapy.[12–14] Zhang *et al.* developed macrocycle-based supramolecular chemotherapy strategies through the inclusion of chemotherapeutic drugs to realize selective damage to tumor cells. CB[7]'s encapsulation reduced guest drug's toxicity towards normal cells, and the cytotoxicity towards cancer cells was recovered *via* competitive displacement of guest drugs with overexpressed spermine inside cancer cells.[15,16] *Via* the covalent conjugation of CB[7] with biotin, targeted delivery of oxaliplatin to cancer cells was achieved, and thus supramolecular chemotherapy efficiency can be further boosted.[17] Moreover, Wang *et al.* reported guest recognition of chemotherapeutic drugs by unoccupied CB[7] that was covalently conjugated onto the surface of Fe_3O_4 and gold nanomaterials, to realize magnetic resonance imaging-guided chemotherapy and computerized tomography-guided synergistic photothermal chemotherapy, respectively.[18,19] Kim *et al.* synthesized Cy3-conjugated CB[7] and investigated its supramolecular latching with adamantane-conjugated Cy5/BDP630/650 and adamantane-labeled protein inside live organisms for the direct observation of dynamic organelle fusion processes, *in vitro* cellular protein and *in vivo* site-specific imaging.[20–22] In addition, live cell imaging was also demonstrated by Urbach *et al.*[23] and Kim *et al.*[24] through direct endocytosis of dye-conjugated CB[7] (Rhodamine and Cy3). However, these traditional dyes harnessed on CB[7] may suffer from severe aggregation-caused quenching (ACQ) in an aqueous environment, which hampered their high-concentration usage, thus impairing the sensitivity for cellular imaging.

Herein we designed an AIEgen functionalized CB[7] (AIECB[7]) *via* a facile "click" reaction between mono-propargyloxy-CB[7] and an azide AIEgen photosensitizer (Scheme S1†), in which the cavity of CB[7] was kept intact. To the best of our knowledge, the covalent conjugation of an AIEgen with CB[7] has never been reported. Through rational selection of the AIEgen, AIECB[7] was endowed with excellent optical properties, such as red-shifted fluorescence and singlet oxygen generation. AIECB[7] may spontaneously form nanoaggregates in an aqueous environment due to its amphiphilicity. Additionally, as CB[7]'s cavity was unoccupied, drug molecules such as oxaliplatin and banoxantrone (AQ4N)[16,25] can be loaded through host–guest recognition of CB[7], to realize imaging-guided synergistic photodynamic therapy and chemotherapy (Scheme 1).

Results and discussion

As shown in Scheme 2, the functionalization of CB[7] started from mono-hydroxylation of CB[7] by following reported procedures,[26] and then mono-hydroxylated CB[7] (CB[7]-OH, Fig. S1†) was transformed into mono-propargyloxy CB[7] (CB[7]-alkyne, Fig. S2–S4†) through a nucleophilic substitution reaction.[27] AIECB[7] was synthesized *via* a CuAAC-catalyzed "click" reaction between CB[7]-alkyne and an azido functionalized fluorescence AIEgen photosensitizer (TPEPy-N_3, Fig. S5–S11†).[28] The reaction solution containing AIECB[7] was dialyzed against Milli-Q water to remove Cu residue from the catalyst (<1 mol%, Fig. S12†). The structure of AIECB[7] was fully characterized by ^{1}H NMR (Fig. S13†), ^{1}H-^{13}C 2D HSQC NMR (Fig. S14†), ESI-MS (high-resolution, Fig. S15†) and FTIR (Fig. S16†). In the ^{1}H NMR spectrum (Fig. S13†), both the

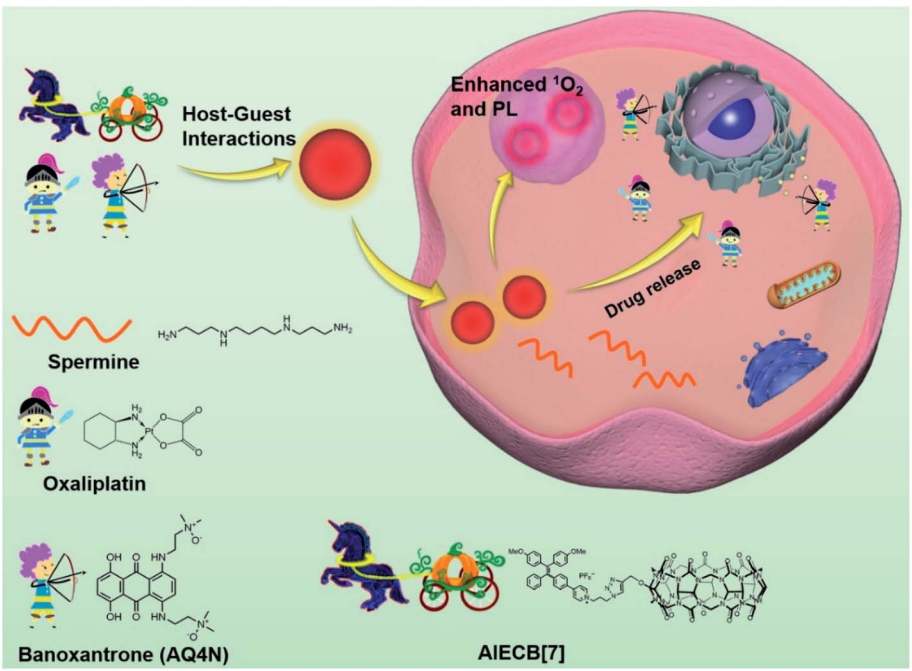

Scheme 1 Schematic illustration of the design of AIECB[7] and its application for imaging-guided, synergistic PDT and supramolecular chemotherapy.

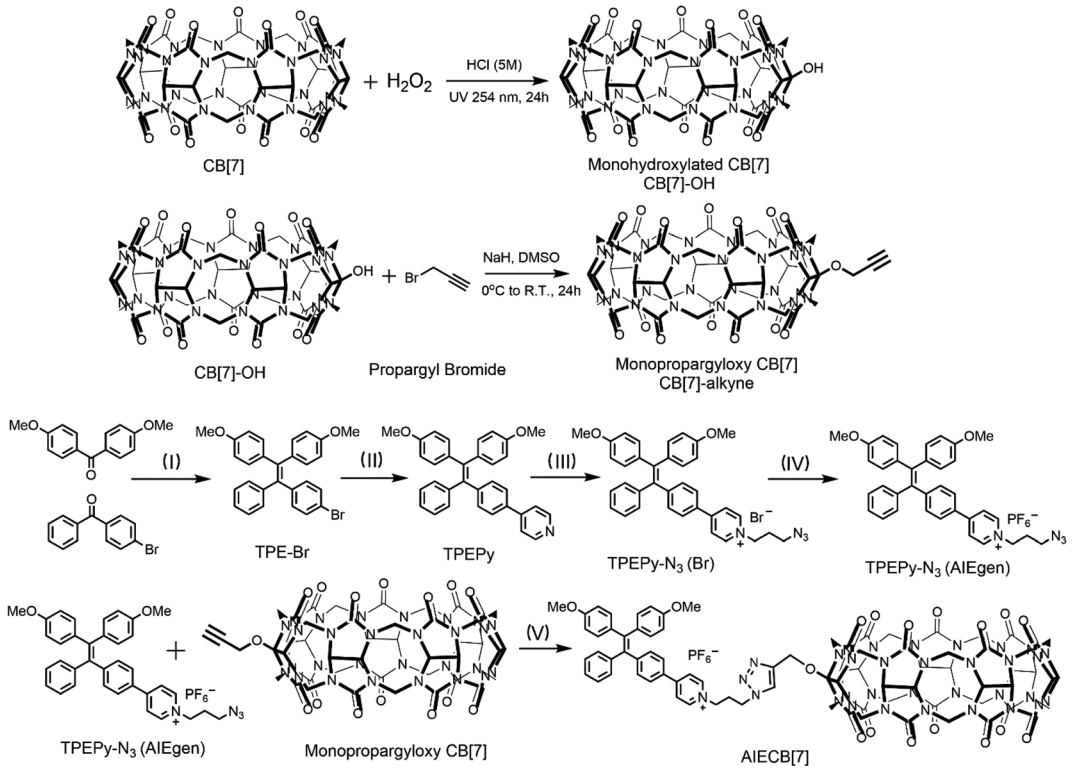

Scheme 2 The Synthetic route for AIECB[7]. Reagents and conditions: (I) $TiCl_4$, Zn dust, anhydrous THF, −78 °C, and 24 h; (II) 4-pyridinylboronic acid, $Pd(PPh_3)_4$, TBAB, 2M K_2CO_3 (aq), THF, 80 °C, and 5 h; (III) 1-azido-3-bromopropane, DMF, 100 °C, and 12 h; (IV) KPF_6; (V) $CuSO_4$, sodium ascorbate, DMSO, 80 °C, and 24 h.

resonance signals corresponding to CB[7] (5.78–5.50 ppm, 5.49–5.20 ppm and 4.25–4.00 ppm) and the aryl groups of the AIEgen (8.33 to 6.74 ppm) were observed, indicating the successful conjugation of the AIEgen with CB[7]. In the FTIR spectrum of AIECB[7] (Fig. S16†), the signals at 2102 cm^{-1} corresponding to the azide group disappeared, indicating the complete consumption of TPEPy-N_3 (AIEgen) with the alkynyl group of CB[7]-alkyne. Additionally, ESI-MS (high-resolution) further verified the covalent connection of AIE with CB[7] (*m*/*z*: [AIECB[7] + 1-adamantanamine hydrochloride]$^{2+}$, calcd for ($C_{91}H_{92}N_{33}O_{17}$), 960.8792; found, 960.8704).

As the main skeleton of AIE is highly hydrophobic and CB[7] is generally hydrophilic, AIECB[7] spontaneously self-assembled in aqueous solution without organic solvent assistance, forming a clear and transparent colloidal solution. The AIECB[7] assemblies exhibited good water stability at room temperature, and 60 μM AIECB[7] was found to remain stable for at least 3 days, determined by DLS measurement (Fig. S17†). The absorption of AIECB[7] exhibited a good linear relationship with concentrations below 60 μM, which obeys the Lambert–Beer law (Fig. S18†). Additionally, little differences were observed in the sizes of AIECB[7] nanoaggregates at concentrations of 10, 20, 40 and 60 μM, based on the DLS results (Fig. S19A†). Both the particle sizes (Fig. S19B†) and PL intensities (Fig. S20†) of AIECB[7] nanoaggregates also showed negligible differences in several biologically relevant media (water, PBS, 0.1× PBS, and saline). As shown in Fig. 1A and S21,† the UV-vis spectrum of AIECB[7] nanoaggregates was similar to that of the AIEgen (TPEPy-N_3), with an identical absorbance profile in the 350–500 nm range. The fluorescence of AIECB[7] was blue-shifted compared with that of the AIEgen (Fig. 1B and S21†), presumably due to the lowered positive charge density on the backbone of the AIEgen,[29,30] resulting from the ion-dipole interaction between the pyridinium cation of the AIEgen and the highly negative carbonyl portals of CB[7].[31,32] At the same time, the fluorescence intensity of AIECB[7] was also modestly compromised, because the bulky CB[7] macrocycle may loosen the tight stacking of AIEgens. Interestingly, in an acidic solution, the fluorescence intensity of AIECB[7] was found to be much higher than that in a neutral solution (Fig. 1B and S22A†), likely due to the weakened interactions between the carbonyl portals of CB[7] and pyridinium cation of the AIEgen by the interruption of H^+ in an acidic environment, leading to the tighter stacking of AIECB[7] assemblies. In contrast, the AIEgen alone was not sensitive to the pH change (from 7.0 to 1.0, Fig. S22B†). The singlet oxygen ($^1O_2$) generation of AIECB[7] assemblies was investigated by employing anthracenediyl-bis(methylene)dimalonic acid (ABDA) as the $^1O_2$ trapper. As shown in Fig. S23† and 1C, the $^1O_2$ generation efficiency of AIECB[7] was much lower in a neutral environment than that in weakly acidic solution that simulates the cancer tissue's microenvironment, exhibiting a similar manner to that of fluorescence intensity. In reference experiments, the CB[7] mixed with the AIEgen and the AIEgen alone did not show

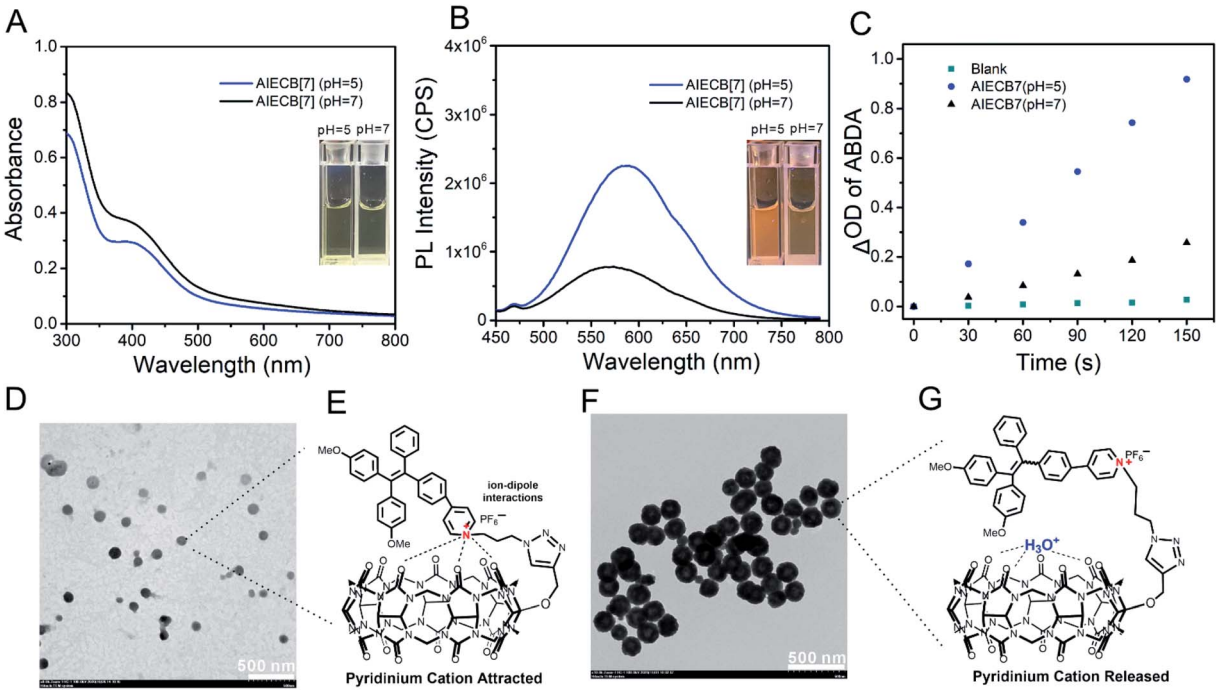

Fig. 1 UV-vis absorbance (A) and fluorescence spectra (B) of AIECB[7] assemblies. The inset images were taken under white light (A) and 365 nm UV light (B), respectively. (C) Singlet oxygen ($^1O_2$) generation of AIECB[7] determined by measuring the absorbance changes of ABDA at 378 nm. Typical TEM images and postulated configurations of AIECB[7] assemblies in aqueous solutions at pH = 7 (D and E) and pH = 5 (F and G), respectively. Scale bars: 500 nm.

considerable differences with pH changes (Fig. S24†), unlike the AIECB[7] nanoaggregates. The relatively lower photo-toxicity in a neutral environment and enhanced photo-toxicity in acidic environments will indeed lead to specific cytotoxicity against cancer cells and tissues during the PDT process.[33] Transmission electron microscopy (TEM) was introduced to investigate the mechanism of the inner aggregation of AIECB[7] nanoaggregates. As shown in Fig. 1D and F, the assemblies of AIECB

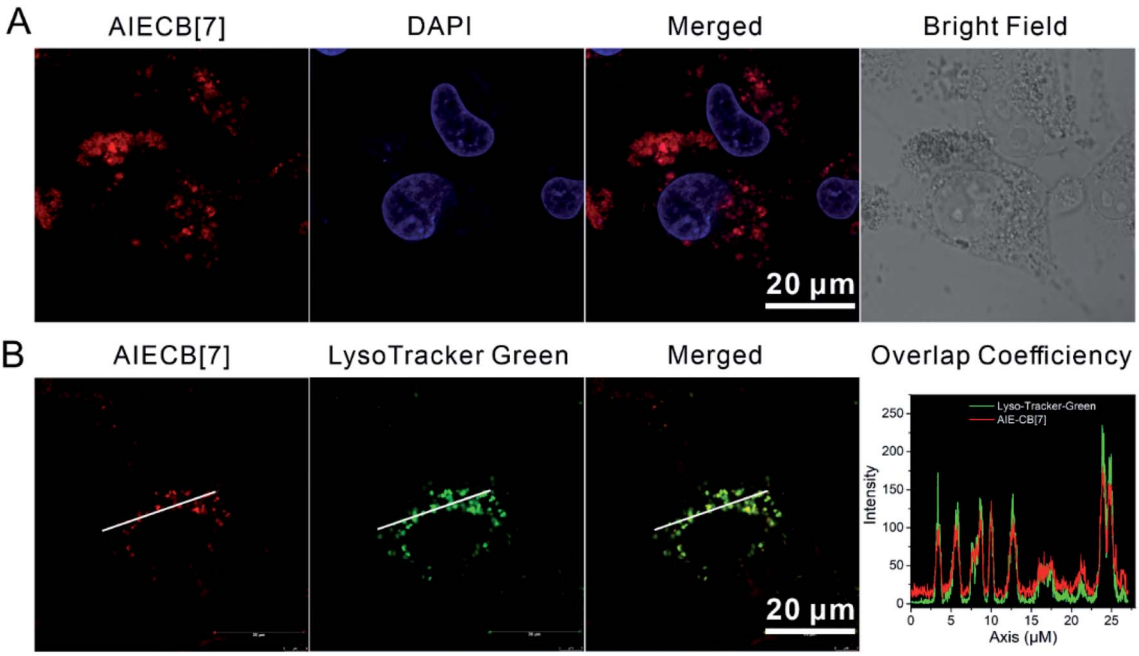

Fig. 2 (A) Cellular internalization of AIECB[7]. The cell nucleus was stained with DAPI. (B) Subcellular localization and overlap coefficiency of AIECB[7] and LysoTracker Green in A549 cells. AIECB[7], Exi: 488 nm, and Emi: 565–660 nm; LysoTracker Green, Exi: 488 nm, and Emi: 495–550 nm. Scale bars: 20 μm. The cellular experiments were performed three independent times.

[7] in an acidic environment were relatively larger and more compact than those in neutral environments, where AIECB[7] nanoaggregates are loosely packed resulting in the presence of many small particles. The hydrodynamic radius of AIECB[7] assemblies from DLS results was also in line with TEM characterization (Fig. S25†), suggesting the possibly different packing configurations of AIECB[7] in neutral and acidic solutions, where acidic conditions may protonate the carbonyl portals of CB[7] and improve the packing of AIEgens (Fig. 1E and G).

The cellular internalization of AIECB[7] was subsequently studied in A549 cells by taking advantage of its inherent fluorescence. As shown in Fig. 2A and S26,† AIECB[7] was efficiently taken up by A549 cells after incubation at 37 °C for 8 h, and it mainly localized in the lysosome. In particular, AIECB[7] displayed enhanced fluorescence specifically in the lysosome (acidic environment, pH = 4.5–5.5)[34] stained with the commercial LysoTracker-Green dye (Fig. 2B). Due to the use of an AIEgen that is resistant to ACQ and resistant to photobleaching, AIECB[7] is expected to exhibit superior subcellular imaging properties than a previous reported CB[7]-dye conjugate.[23,24]

Singlet oxygen ($^1O_2$) is highly cytotoxic to cells and responsible for the PDT mediated cellular apoptosis. As shown in Fig. S27,† the irradiation of A549 cells treated with AIECB[7] with 450 nm light at 100 mW cm^{-2} for 1 min led to significant intracellular $^1O_2$ (stained with DCFH_DA). Interestingly, by prolonging the time of irradiation to 3 min, the cell membrane of A549 cells started to bud and then evolved into membrane vesicles (Fig. S28†). Meanwhile, the cytoskeletons also gradually collapsed, suggesting that an aggressive cell apoptosis process was taking place. As shown in Fig. 3, upon staining with Annexin-V FITC/PI, intense fluorescence of FITC and PI was observed in AIECB[7] treated cells that were irradiated with

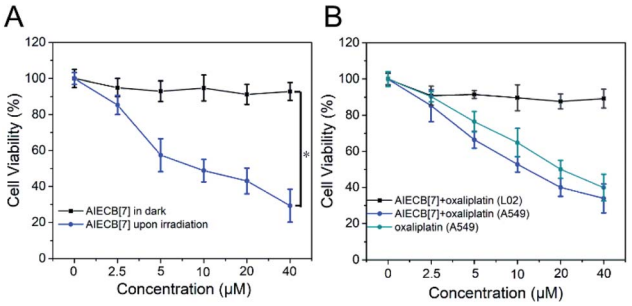

Fig. 4 (A) The cell viabilities of A549 incubated with AIECB[7] upon 450 nm light irradiation and in the dark. (B) The cell viabilities of LO2 and A549 incubated with AIECB[7] + oxaliplatin and oxaliplatin alone, respectively. All the measurements were performed three independent times. *$P < 0.05$ compared to AIECB[7] in the dark group obtained by using Student's t-test.

450 nm light (150 mW cm^{-2} for 4 min), indicating PDT induced cellular apoptosis. In contrast, negligible fluorescent signals were observed in the control groups of cells. Meanwhile, when AIECB[7] treated A549 cells were co-incubated with reductive L-ascorbic acid sodium salt (NAC), the cell apoptosis process was effectively inhibited (Fig. 3, last column), implying that the cell apoptosis process was induced by $^1O_2$ mediated PDT.

Next, the biocompatibility and therapeutic efficacy of AIECB[7] were assessed *in vitro via* MTT assays. A549 cells were incubated with AIECB[7] (2.5 to 40 μM) and were subsequently treated with and without 450 nm light irradiation (150 mW cm^{-2}) for 4 min, respectively. As shown in Fig. 4A, AIECB[7] showed negligible cytotoxicity in the absence of light irradiation even at a concentration of 40 μM, suggesting the high biocompatibility of this material. However, the IC_{50} of AIECB[7] against A549 cells was determined to be *ca.* 10 μM when irradiated with 450 nm light, indicative of effective PDT of AIECB

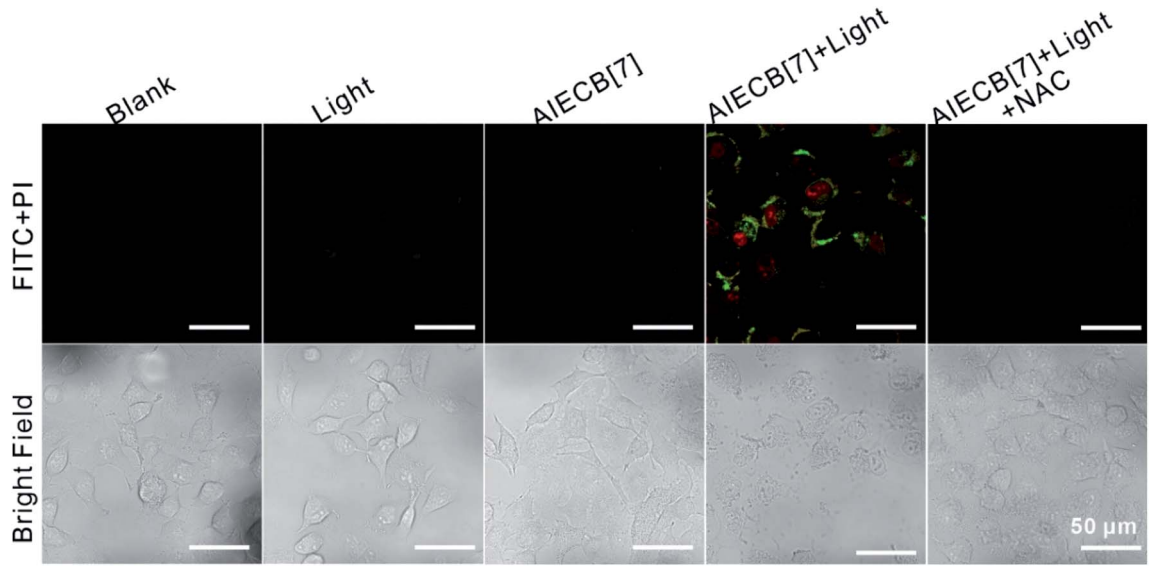

Fig. 3 CLSM images of Annexin V-FITC/PI stained A549 cells with various treatments. Scale bars: 50 μm. The cellular experiments were performed three independent times.

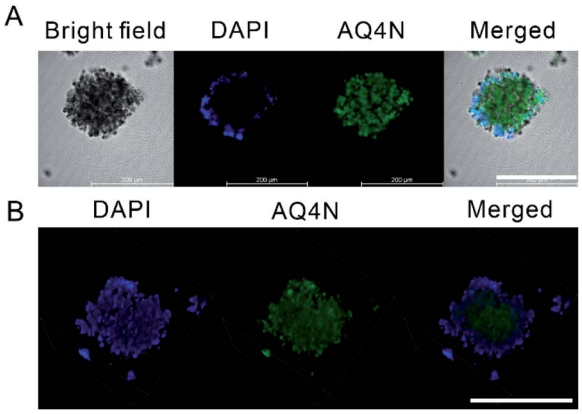

Fig. 5 2D Images (A) and Z-stack scanning images (3D version, B) of A549 tumor spheroids treated with AIECB[7] + AQ4N and stained with DAPI to detect the penetration of AQ4N. Scale bars: 200 μm. The cellular experiments were performed three independent times.

[7], attributed to efficient cellular internalization and high singlet oxygen generation efficiency.

To leverage the guest-binding properties of CB[7] from AIECB[7] for potential supramolecular chemotherapy on the top of PDT, oxaliplatin was loaded into AIECB[7] *via* CB[7]-oxaliplatin host–guest interactions.[35] The loading efficiency of oxaliplatin was assessed to be *ca.* 96.3% in molar percentage of CB[7], determined by ICP-MS analysis. As shown in Fig. 4B, AIECB[7] + oxaliplatin exhibited negligible toxicity to LO2 (human hepatic cell) cells at concentrations from 2.5 to 40 μM in the dark, as the oxaliplatin was encapsulated by CB[7] and could not be released efficiently.[15] Conversely, AIECB[7] + oxaliplatin killed about 65% of A549 cells at a concentration of 40 μM, due to the release of oxaliplatin in A549 cells *via* competitive replacement by spermine that is overexpressed in this cell line.[36] Additionally, AIECB[7] + oxaliplatin showed a comparable, or even moderately better, antitumor efficacy than free oxaliplatin (p value of 0.63), likely due to the improved cellular uptake by the nanocarrier.[16,37] As expected, AIECB[7] alone in the dark or light did not lead to obvious apoptosis, confirming the high biocompatibility of AIECB[7] and safe power density of the applied light, as shown in Fig. S29.† In contrast, remarkable cellular apoptosis was observed in the PDT treated group by AIECB[7] under light irradiation or in the chemotherapy group by oxaliplatin. Significantly, an extraordinarily higher anticancer activity was observed in the group treated with AIECB[7] + oxaliplatin upon light irradiation, when compared respectively to the PDT and chemotherapy groups, due to the synergistic effects from PDT and chemotherapy.

Inspired by the synergistic effects of PDT chemotherapy, a hypoxia-activatable prodrug, banoxantrone (AQ4N), was employed to cooperate with the O_2-depleting PDT process.[38,39] An A549 multicellular tumor spheroid (MCTS) model was established to mimic the hypoxic solid tumors, which is widely used as a high throughput screening platform for anticancer drug discovery and development.[40,41] After 24 h, AQ4N in the form of AIECB[7] + AQ4N fully penetrated into the tumor spheroid as shown in Fig. 5 and Fig. S30,† suggesting that the nanoaggregates may deliver AQ4N into the deep tumor spheroid region. Subsequently, the *in vitro* anti-tumor efficacy of AIECB[7] + AQ4N, AIECB[7] and free AQ4N was respectively investigated using these MCTS models. As shown in Fig. 6A and Fig. S31,† thorough apoptosis was observed in the core of MCTS treated by AIECB[7] + AQ4N, indicating that the intratumoral hypoxic environment successfully activated the cytotoxicity of AQ4N. Furthermore, with the extension of treatment time, a heavier damage to the MCTS was observed (Fig. S32†). In contrast, many cancer cells survived in the MCTS treated with only the AIECB[7] group *via* the PDT approach (Fig. 6A),

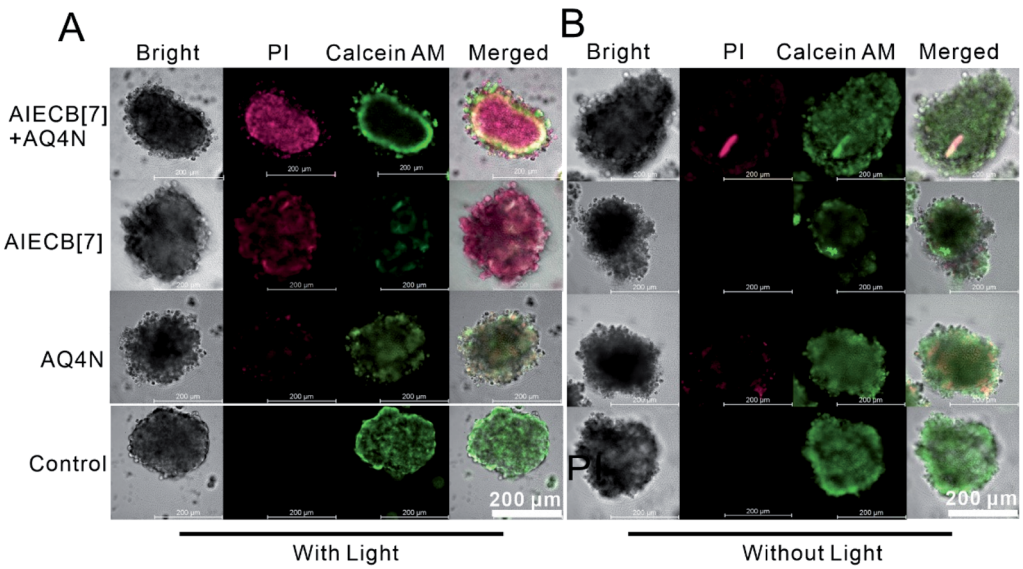

Fig. 6 Cell viabilities of A549 tumor spheroids after being treated with AIECB[7] + AQ4N, AIECB[7] and AQ4N respectively with (A) and without (B) light irradiation. Scale bars: 200 μm. The green fluorescence of Calcein AM and red fluorescence of PI indicate living cells and dead cells, respectively. The cellular experiments were performed three independent times.

indicating that PDT alone could not effectively kill tumor cells inside hypoxic tumor tissue due to the lack of sufficient oxygen for singlet oxygen generation. Meanwhile, free AQ4N alone exhibited very modest cytotoxicity in the presence (Fig. 6A) or absence (Fig. 6B) of light irradiation in the MCTS model, due to its poor tissue penetration. Taken together, AQ4N loaded AIECB[7] exhibited synergistic anti-tumor activities *in vitro*, as a consequence of PDT and hypoxia-activated supramolecular chemotherapy.

Conclusions

In summary, we synthesized a fluorescent AIE-photosensitizer functionalized CB[7] derivative, namely AIECB[7], which could spontaneously self-assemble into nanoaggregates in an aqueous solution for bioimaging and photodynamic therapy. Interestingly, in response to weakly acidic conditions, the intramolecular stacking of AIECB[7] was regulated into a more compact form, leading to enhanced fluorescence emission and singlet oxygen generation. In addition, AIECB[7] nanoaggregates specifically lit up lysosomes and exhibited enhanced photodynamic cytotoxicity against cancer cells *in vitro*. Thanks to the presence of CB[7], chemotherapeutic drugs (*e.g.* oxaliplatin and AQ4N) were respectively loaded into CB[7] of AIECB[7] nanoaggregates *via* host–guest interactions to realize synergistic chemo-photodynamic therapy. This work not only provides unprecedented AIECB[7] for versatile theranostic applications, but also offers important new insights into the design and development of macrocycle-conjugated AIE materials that allow for modular modification for diverse biomedical applications.

Author contributions

Jia Chen: investigation, validation, writing – original draft, formal analysis, data curation. Shengke Li: validation, formal analysis, data curation, writing – review, Zeyu Wang: investigation, visualization, Yating Pan: investigation, visualization, Jianwen Wei: formal analysis, data curation, Siyu Lu: investigation, validation, Qing-Wen Zhang: methodology, Lian-Hui Wang: conceptualization, methodology, Ruibing Wang: conceptualization, methodology, writing – review & editing, supervision, funding acquisition, supervision, resources.

Conflicts of interest

There are no conflicts to declare.

Acknowledgements

This work was financially supported by the Science and Technology Development Fund (FDCT), Macau SAR (0121/2018/A3, 0007/2020/A, and SKL-QRCM(UM)-2020–2022), and National Natural Science Foundation of China (22071275 and 21871301). Jia Chen is grateful to the financial support of the UM Macao Postdoctoral Associateship under the UM Macao Talent Program. We are also grateful to the Proteomics, Metabolomics and Drug Development Core, Faculty of Health Sciences, University of Macau, for the support with the molecular mass characterization.

Notes and references

1 J. Mei, N. L. Leung, R. T. Kwok, J. W. Lam and B. Z. Tang, *Chem. Rev.*, 2015, **115**, 11718–11940.
2 Kenry, B. Z. Tang and B. Liu, *Chem*, 2020, **6**, 1195–1198.
3 X.-Y. Lou and Y.-W. Yang, *Aggregate*, 2020, **1**, 19–30.
4 S. Xu, W. Wu, X. Cai, C. J. Zhang, Y. Yuan, J. Liang, G. Feng, P. Manghnani and B. Liu, *Chem. Commun.*, 2017, **53**, 8727–8730.
5 S. Xu, Y. Yuan, X. Cai, C. J. Zhang, F. Hu, J. Liang, G. Zhang, D. Zhang and B. Liu, *Chem. Sci.*, 2015, **6**, 5824–5830.
6 X. H. Wang, N. Song, W. Hou, C. Y. Wang, Y. Wang, J. Tang and Y. W. Yang, *Adv. Mater.*, 2019, **31**, 1903962.
7 D. Dai, Z. Li, J. Yang, C. Wang, J. R. Wu, Y. Wang, D. Zhang and Y. W. Yang, *J. Am. Chem. Soc.*, 2019, **141**, 4756–4763.
8 C. Chen, X. Ni, H. W. Tian, Q. Liu, D. S. Guo and D. Ding, *Angew. Chem., Int. Ed.*, 2020, **59**, 11779–11783.
9 L. Shao, Y. Pan, B. Hua, S. Xu, G. Yu, M. Wang, B. Liu and F. Huang, *Angew. Chem., Int. Ed.*, 2020, **59**, 11779–11783.
10 Y. Li, Y. Dong, X. Miao, Y. Ren, B. Zhang, P. Wang, Y. Yu, B. Li, L. Isaacs and L. Cao, *Angew. Chem., Int. Ed.*, 2018, **57**, 729–733.
11 Y. Li, C. Qin, Q. Li, P. Wang, X. Miao, H. Jin, W. Ao and L. Cao, *Adv. Opt. Mater.*, 2020, **8**, 1902154.
12 X. Yang, R. Wang, A. Kermagoret and D. Bardelang, *Angew. Chem., Int. Ed.*, 2020, **59**, 21280–21292.
13 J. Lagona, P. Mukhopadhyay, S. Chakrabarti and L. Isaacs, *Angew. Chem., Int. Ed.*, 2005, **44**, 4844–4870.
14 S. Li, Y. Gao, Y. Ding, A. Xu and H. Tan, *Chin. Chem. Lett.*, 2021, **32**, 313–318.
15 Y. Chen, Z. Huang, H. Zhao, J. F. Xu, Z. Sun and X. Zhang, *ACS Appl. Mater. Interfaces*, 2017, **9**, 8602–8608.
16 H. Chen, Y. Chen, H. Wu, J. F. Xu, Z. Sun and X. Zhang, *Biomaterials*, 2018, **178**, 697–705.
17 L. Cao, G. Hettiarachchi, V. Briken and L. Isaacs, *Angew. Chem., Int. Ed.*, 2013, **52**, 12033–12037.
18 L. Yue, C. Sun, C. H. T. Kwong and R. Wang, *J. Mater. Chem. B*, 2020, **8**, 2749–2753.
19 L. Yue, C. Sun, Q. Cheng, Y. Ding, J. Wei and R. Wang, *Chem. Commun.*, 2019, **55**, 13506–13509.
20 M. Li, A. Lee, K. L. Kim, J. Murray, A. Shrinidhi, G. Sung, K. M. Park and K. Kim, *Angew. Chem., Int. Ed.*, 2018, **57**, 2120–2125.
21 M. Li, S. Kim, A. Lee, A. Shrinidhi, Y. H. Ko, H. G. Lim, H. H. Kim, K. B. Bae, K. M. Park and K. Kim, *ACS Appl. Mater. Interfaces*, 2019, **11**, 43920–43927.
22 K. L. Kim, G. Sung, J. Sim, J. Murray, M. Li, A. Lee, A. Shrinidhi, K. M. Park and K. Kim, *Nat. Commun.*, 2018, **9**, 1712–1721.
23 A. T. Bockus, L. C. Smith, A. G. Grice, O. A. Ali, C. C. Young, W. Mobley, A. Leek, J. L. Roberts, B. Vinciguerra, L. Isaacs and A. R. Urbach, *J. Am. Chem. Soc.*, 2016, **138**, 16549–16552.

24 M. Li, A. Lee, S. Kim, A. Shrinidhi, K. M. Park and K. Kim, *Org. Biomol. Chem.*, 2019, **17**, 6215–6220.
25 A. Buczkowski, P. Tokarz, A. Stepniak, J. Lewkowski, A. Rodacka and B. Palecz, *J. Mol. Liq.*, 2019, **290**, 111190–111197.
26 C. Sun, H. Zhang, S. Li, X. Zhang, Q. Cheng, Y. Ding, L. H. Wang and R. Wang, *ACS Appl. Mater. Interfaces*, 2018, **10**, 25090–25098.
27 C. Hu, L. Grimm, A. Prabodh, A. Baksi, A. Siennicka, P. A. Levkin, M. M. Kappes and F. Biedermann, *Chem. Sci.*, 2020, **11**, 11142–11153.
28 G. Qi, F. Hu, Kenry, L. Shi, M. Wu and B. Liu, *Angew. Chem., Int. Ed.*, 2019, **58**, 16229–16235.
29 W. Wu, D. Mao, S. Xu, S. Ji, F. Hu, D. Ding, D. Kong and B. Liu, *Mater. Horiz.*, 2017, **4**, 1110–1114.
30 W. Wu, D. Mao, F. Hu, S. Xu, C. Chen, C. J. Zhang, X. Cheng, Y. Yuan, D. Ding, D. Kong and B. Liu, *Adv. Mater.*, 2017, **29**, 1700548.
31 E. Masson, X. Ling, R. Joseph, L. Kyeremeh-Mensah and X. Lu, *RSC Adv.*, 2012, **2**, 1213–1247.
32 F. Biedermann and H. J. Schneider, *Chem. Rev.*, 2016, **116**, 5216–5300.
33 X. Li, J. F. Lovell, J. Yoon and X. Chen, *Nat. Rev. Clin. Oncol.*, 2020, **17**, 657–674.
34 Z. Dong, Q. Han, Z. Mou, G. Li and W. Liu, *J. Mater. Chem. B*, 2018, **6**, 1322–1327.
35 Y. Jin Jeon, S.-Y. Kim, Y. Ho Ko, S. Sakamoto, K. Yamaguchi and K. Kim, *Org. Biomol. Chem.*, 2005, **3**, 2122–2125.
36 E. W. Gerner and F. L. Meyskens, *Nat. Rev. Cancer*, 2004, **4**, 781–792.
37 Q. Hao, Y. Chen, Z. Huang, J. F. Xu, Z. Sun and X. Zhang, *ACS Appl. Mater. Interfaces*, 2018, **10**, 5365–5372.
38 L. H. Patterson and S. R. McKeown, *Br. J. Cancer*, 2000, **83**, 1589–1593.
39 Z. He, Y. Dai, X. Li, D. Guo, Y. Liu, X. Huang, J. Jiang, S. Wang, G. Zhu, F. Zhang, L. Lin, J.-J. Zhu, G. Yu and X. Chen, *Small*, 2019, **15**, 1804131.
40 E. C. Costa, A. F. Moreira, D. de Melo-Diogo, V. M. Gaspar, M. P. Carvalho and I. J. Correia, *Biotechnol. Adv.*, 2016, **34**, 1427–1441.
41 W. Shi, J. Kwon, Y. Huang, J. Tan, C. G. Uhl, R. He, C. Zhou and Y. Liu, *Sci. Rep.*, 2018, **8**, 6837–6846.